Electrochimica Acta 55 (2010) 3628–3633

Contents lists available at ScienceDirect

Electrochimica Acta

journal homepage: www.elsevier.com/locate/electacta

Additive treatment effect of TiO_2 as supports for Pt-based electrocatalysts on oxygen reduction reaction activity

Dae-Suk Kim, Essam F. Abo Zeid, Yong-Tae Kim*

School of Mechanical Engineering, Pusan National University, Jangjeon-dong, Geumjeong-gu, Busan 609-735, Republic of Korea

ARTICLE INFO

Article history:
Received 17 September 2009
Received in revised form
28 December 2009
Accepted 14 January 2010
Available online 25 January 2010

Keywords:
Polymer electrolyte membrane fuel cell (PEMFC)
Cathode electrocatalyst
Oxygen reduction reaction
Oxide support
TiO_2

ABSTRACT

In this study, we investigated the additive treatment effect of TiO_2 as alternative support materials to common carbon black for Pt-based electrocatalysts on electrocatalytic activity for oxygen reduction reaction (ORR). The shape of TiO_2 was varied by hydrothermal treatment with various additives, such as urea, thiourea, and hydrofluoric acid. From the results of transmission electron microscopy (TEM) images and ultraviolet–visible spectroscopy (UV–vis) spectra, it was identified that the morphology of hydrofluoric acid (HF)-treated TiO_2 was changed into a round shape having lower aspect ratio than other samples, and its band gap was decreased. Notably, the electronic state of HF-treated TiO_2 support was changed into highly reduced (electron rich) state which led to the increase of ORR activity, compared to other samples treated with different additives or before treatment. The electrocatalytic characteristics changes after treatment with various additives were investigated by using X-ray diffraction (XRD), X-ray photoemission spectroscopy (XPS), cyclic voltammograms (CV), and rotating disk electrode (RDE) techniques.

1. Introduction

The polymer electrolyte membrane fuel cell (PEMFC) has been recognized as the most suitable power source to replace the internal combustion engine for transportation applications due to its eco-friendly system and high power density [1]. However, the reliability of PEMFC must be improved before commercialization of fuel cell electric vehicles (FCEV) becomes practical. Approximately 5500 h of fuel cell operation is required for a FCEV, and the oxygen reduction reaction (ORR) activity of the cathode electrocatalyst strongly affects PEMFC performance and long-term stability [2]. Carbon materials are usually employed as the supports for platinum or platinum alloy-based electrocatalysts because it has high-surface area and good electronic conductivity [3–6]. A main drawback is, however, carbon corrosion at the cathode site in which the electrode potential and pH are relatively high. As carbon is eroded away, noble metal nanoparticles can be lost from the electrode or lumped into larger particles. This may cause the deterioration of both catalytic activity and stability; alternative carbon supports which have high durability are therefore required for practical fuel cell operation [7].

In recent, the studies on oxide supports as alternative materials to carbon supports have been carried out to enhance the durability of electrocatalysts and reported that oxide supports showed better corrosion resistance and lower degradation of active surface area [8–15]. Among the many possible oxides, a considerable attention has been paid to TiO_2 materials for durable supports with its suitable characteristics in PEMFC operation condition, such as low cost, commercial availability, stability in water, and the facility to control size and structure [16–21].

Unfortunately, TiO_2 materials are semiconductors having wide band gaps of 3.0 eV for rutile and 3.2 eV for anatase structure [22–24], the improvement of electronic conductivity is therefore required to apply them to actual electrocatalyst supports.

In this paper, we demonstrated a unique method to change the electronic characteristics of TiO_2 supports based on a hydrothermal treatment with various additives which gave rise to a drastic change of their morphology. The change of electrocatalytic activity were finally investigated by using ultraviolet–visible spectroscopy (UV–vis), transmission electron microscopy (TEM), X-ray diffraction (XRD), X-ray photoemission spectroscopy (XPS), and cyclic voltammograms (CV) with rotating disk electrode (RDE).

2. Experimental

2.1. Catalysts synthesis

Four kinds of additive-treated TiO_2 support samples were obtained via the hydrothermal reaction with various additives. At first, rutile TiO_2 (2 g, Aldrich) was mixed in 90 ml of deionized

* Corresponding author. Tel.: +82 51 510 1012; fax: +82 51 514 0685.
E-mail address: yongtae@pusan.ac.kr (Y.-T. Kim).

0013-4686/$ – see front matter.
doi:10.1016/j.electacta.2010.01.055

(DI) water with sonication. Followed by the dissolution of TiO_2, the hydrothermal reaction was conducted at 200 °C with rotation at 150 rpm for 24 h, with urea (0.86 g, Kanto Chemical), thiourea (0.95 g, Kanto Chemical), and hydrofluoric acid (0.747 ml, J.T. Baker) or without any additives. After the reaction, the precipitate was filtered and washed with DI water and ethanol several times, and then, samples were dried at 70 °C. The non-additive-treated TiO_2 is referred to as TiO_2 (non), and additive-treated TiO_2 in urea, thiourea, and hydrofluoric acid (HF) is as TiO_2 (urea), TiO_2 (thiourea), and TiO_2 (HF), respectively.

Pt electrocatalysts supported on additive-treated TiO_2 supports were prepared with the borohydride reduction method. Additive-treated TiO_2 supports and $H_2PtCl_6{\cdot}6H_2O$ (support weight 20 wt.% of Pt) were dissolved in DI water with sonication. To reduce the Pt precursor, $NaBH_4$ dissolved in DI water was rapidly dropped into the solution with vigorous stirring for 12 h. The precipitate was filtered and washed several times with DI water and ethanol. After evaporation and drying, Pt electrocatalysts supported on the additive-treated TiO_2 were obtained, which were referred to in this paper as Pt/TiO_2 (non), Pt/TiO_2 (urea), Pt/TiO_2 (thiourea), and Pt/TiO_2 (HF).

2.2. Catalyst characterization

The morphology of electrocatalyst samples was observed by using transmission electron microscopy (TEM, JEOL JEM-2011). Specimens for TEM observation were prepared by placing a drop of the particle-dispersed ethanol solution onto a copper grid; then, the TEM was operated at an accelerating voltage of 200 keV. All images were taken by a charge-coupled device (CCD) camera.

The absorbance spectra of TiO_2 were recorded on a double beam UV–vis spectrophotometer (Scinco SD-1000). Ethanol was used as the reference beam data, and various TiO_2 samples dispersed in ethanol were used as the sample beam data. The spectra were taken from 200 nm to 1000 nm at room temperature.

X-ray photoemission spectroscopy (XPS, ESCALAB250) spectra were obtained to confirm the electronic state of Pt and Ti as well as elemental. The X-ray source was Al Kα with energy of 1486.6 eV operating at 15 kV and 150 W, and the spot size was 500 μm. The resulting binding energies were calibrated to the C1s (284.6 eV) peak.

X-ray diffraction (XRD, Philips Panalytical) measurements of the Pt/TiO_2 electrocatalysts were carried out using Cu Kα radiation (λ = 1.5406 Å). The XRD spectra were obtained using high resolution in the step-scanning mode with a counting time of 50 s per 0.05°. Scans were recorded in the 2θ range of 10–95°. Scherrer's equation was used to estimate the particle size from the XRD results. For this purpose, the (1 1 1) peak of the Pt face-centered cubic (FCC) structure on $2\theta = 40°$ was selected.

2.3. Electrochemical measurements

All electrochemical measurements were performed in a three-electrode electrochemical cell on a potentiostat (Biologic VSP) at room temperature. A thin-layer rotating disk electrode (5 mm in diameter) was used as a working electrode, which was polished with Al_2O_3 slurries and washed in DI water with sonication before the experiments. Well dispersed Pt/TiO_2 (2.5 mg) and carbon black (1.5 mg, Alfa Aesar) as conductors by an ultrasonicator in DI water were deposited onto a glassy carbon electrode by dropping 20 μl of electrocatalysts ink with a micropipette, resulting in Pt loading in 25.48 $\mu g/cm^2{}_{electrode}$. Uniform and thin Pt/TiO_2 + carbon black electrocatalyst layer on the glassy carbon electrode were obtained by mild evaporation and drying at room temperature. Nafion solution (0.025 wt.%, 20 μl) was dropped onto the electrocatalysts coated electrode and dried in a vacuum oven at 70 °C for 30 min. Finally, we

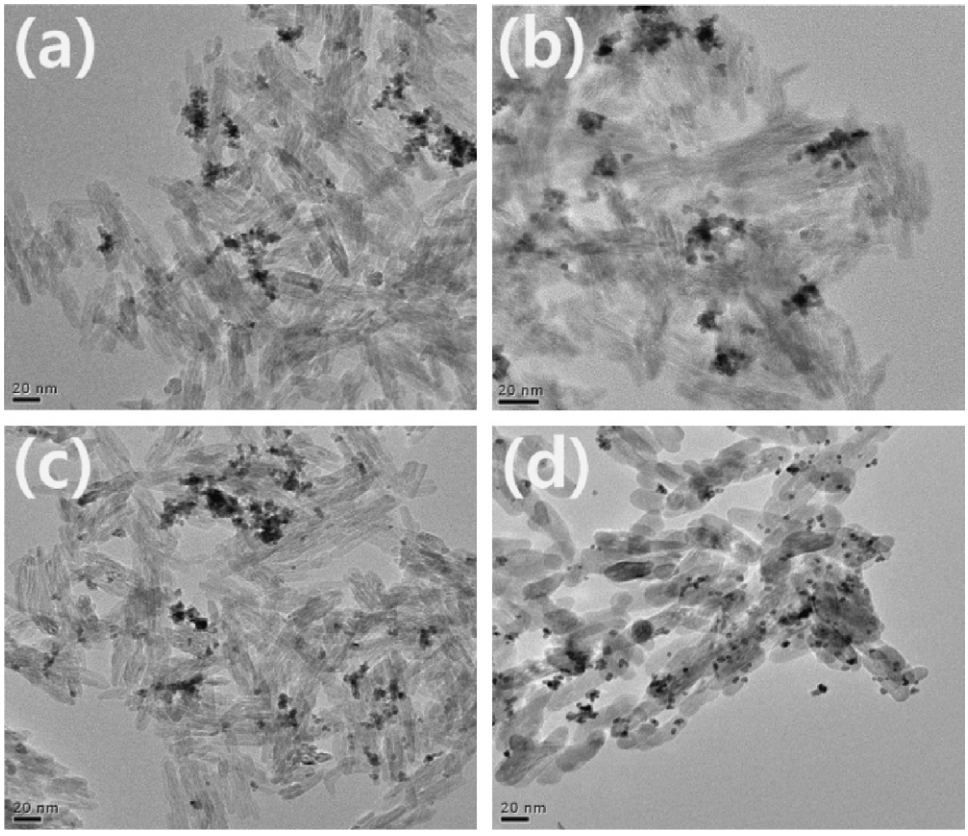

Fig. 1. Representative TEM images of Pt nanoparticles on (a) TiO_2 (non), (b) TiO_2 (urea), (c) TiO_2 (thiourea), and (d) TiO_2 (HF).

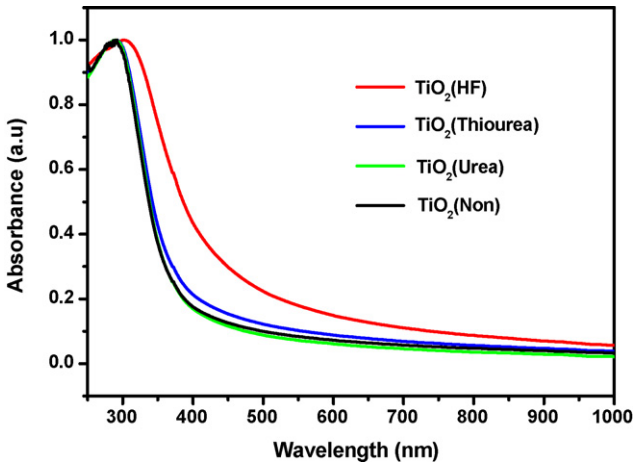

Fig. 2. UV–visible diffuse reflectance spectrum of the various TiO_2 samples.

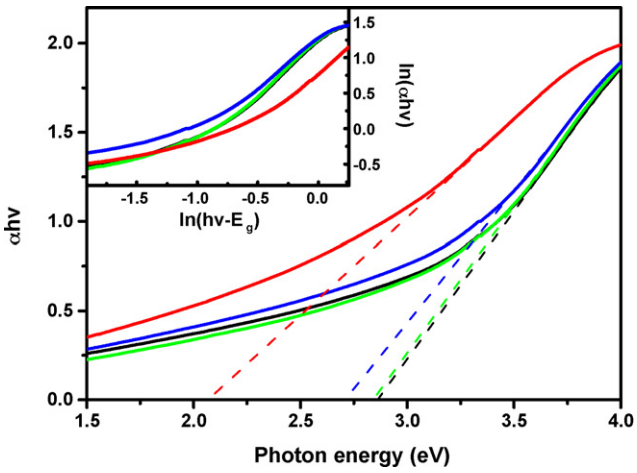

Fig. 3. Plot of determining band gap energy of the various TiO_2 samples. The insert is a plot of $\ln(\alpha h\nu)$ vs. $\ln(h\nu - E_g)$.

could obtain the electrode coated with uniform and thin electocagtalysts layer for thin film rotating disk electrode (TF-RDE) technique. A platinum wire and a silver chloride electrode (Ag/AgCl sat 3.5 M KCl) were used as a counter and a reference electrode, respectively. Cyclic voltammetry (CV) measurements were performed in O_2-free 0.1 M $HClO_4$ electrolyte obtained by purging high-purity N_2 gas for 30 min. The electrodes were cycled in the potential range between −0.195 and 1.005 V versus Ag/AgCl at a scan rate of 20 mV/s after electrochemical cleaning with a quick scan (scan rate: 200 mV/s) for 50 cycles. After CV measurements, oxygen reduction reaction (ORR) was subsequently performed in the same potential range in oxygen-saturated 0.1 M $HClO_4$ by purging pure O_2 gas at rotating speeds of 100, 400, 900, 1600, and 2500 rpm with a scan rate of 5 mV/s. All of the current densities were normalized to the geometric area of the rotating disk electrode.

3. Results and discussion

Fig. 1 shows the TEM images of Pt-based electrocatalysts supported on the additive-treated TiO_2 supports. TiO_2 (non) supports have a nano-stick shape, and the supported Pt nanoparticles were aggregated. In Fig. 1(b and c), the shape of TiO_2 (urea) and TiO_2 (thiourea) was similar to TiO_2 (non), but the Pt nanoparticles were more dispersed than on the TiO_2 (non) sample. An interesting point shown in Fig. 1(d) is that TiO_2 (HF) has more round shapes and Pt nanoparticles were more uniformly dispersed with a smaller particle size than any other samples. Beranek et al. reported that florine (F^-) contained substance affected the morphology and characteristics of TiO_2 [25,26]. Hence, the HF was identified as the most efficient additive to change the shape of TiO_2 in hydrothermal treatment.

The absorbance spectra of TiO_2 were recorded on a double beam UV–vis spectrophotometer to measure the band gap of additive-treated TiO_2. The UV–visible diffuse reflectance spectrum of the various TiO_2 samples is shown in Fig. 2. The optical absorption near the band edge energy follows the relation

$$\alpha h\nu = A \times (h\nu - E_g)^{n/2}, \quad (1)$$

where α, ν, A, and E_g are the absorption coefficient, light frequency, proportionality constant, and band gap, respectively. In Eq. (1), n determines the characteristic of a semiconductor. $n = 1$ for a direct band gap semiconductor and $n = 4$ for an indirect band gap semiconductor. The values of n and E_g were determined by the following steps: first, we plotted $\ln(\alpha h\nu)$ vs. $\ln(h\nu - E_g)$ using an approximate value of E_g, and then determined the value of n from the slope of the straight line. Second, we plotted $(\alpha h\nu)^{2/n}$ vs. $h\nu$ and determined band gap E_g by extrapolating the straight line to the $h\nu$ axis intercept [27–30]. Using this method, the value of n for the oxide was approximately 4 based on the inset of Fig. 3, hence, all the TiO_2 supports treated with various additives are the indirect band gap semiconductors. As can be seen in Fig. 3, the calculated band gaps for TiO_2 (non), TiO_2 (urea), TiO_2 (thiourea), and TiO_2 (HF) were 2.87, 2.85, 2.71, and 2.07 eV, respectively.

Consequently, the optical absorption edges of the additive-treated TiO_2 samples were shifted to the lower energy region compared to the non-additive TiO_2. Notably, it was revealed that HF was the best additive for the shape change into lower aspect ratio, which resulted in the band gap decrease. This result is remarkably consistent with previous studies. Wautelet and co-workers reported that the energy band gap of a TiO_2 semiconductor was affected by the nano-structure of shape and size [31], and this shape change is a key factor in changing the electronic structure of TiO_2 supports. The hydrofluoric acid treatment can be therefore another effective method to decrease the band gap of TiO_2 semiconductor.

The electronic state of the additive-treated TiO_2 supports for Pt-based electrocatalysts were investigated by X-ray photoelectron spectroscopy (XPS). Fig. 4 shows the Pt4f peak (a) and the Ti2p peak (b) of the additive-treated TiO_2 supports for the Pt-based electrocatalysts. The obtained binding energies were calibrated to the C1s (284.6 eV) peak. Through the survey scan, TiO_2 samples were not doped by various additives. It is believed that doping was not taken because complete TiO_2 rutile power was used instead of a Ti precursor in the sample preparation. The Pt4f peak showed similar results for all samples, which indicated that there was no remarkable difference in electronic state of Pt supported on additive-treated TiO_2. However, for the Pt/TiO_2 (HF) sample, the Ti2p peak shifted to the lower binding energy which corresponded to the electron reach state shown in Fig. 4b. This implies that Ti ion in TiO_2 (HF) is in more electron rich phase which can be the origin of the band gap decrease. Table 1 shows the curve fitting results of XPS $Ti2p_{3/2}$ and $Ti2p_{1/2}$ core peaks for various Pt/TiO_2 samples. It was clearly shown that all the additive-treated TiO_2 samples had a small shoulder at lower binding energy than main peak corresponding to more reduced Ti^{2+} or Ti^{3+} state as well as a dominant Ti^{4+} peak. Especially, Pt/TiO_2 (HF) has the highest relative intensity of Ti^{2+} or Ti^{3+} state, which can act as a electron donor and thereby improve the electronic characteristics on the surface of TiO_2 supports.

Fig. 5 shows the XRD analysis of the various Pt/TiO_2 catalysts. All the diffraction peaks show (1 1 1), (2 0 0), (2 2 0), and (3 1 1) of the FCC crystal lattice of platinum. The average particle size of the Pt catalyst supported on the additive-treated TiO_2 was calculated

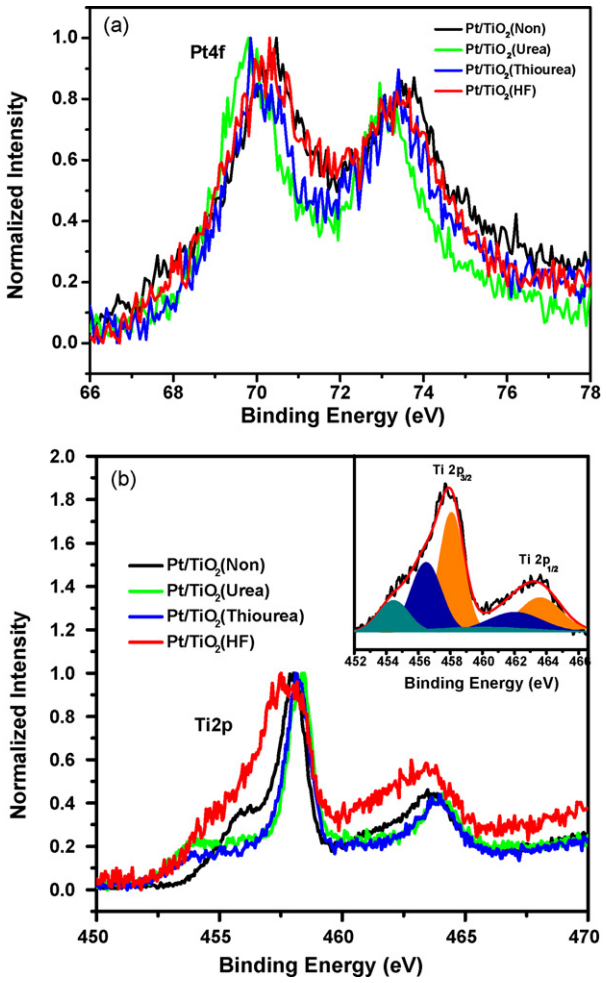

Fig. 4. XPS spectra for (a) Pt4f peak and (b) Ti2p peak of the various Pt/TiO_2 samples. The insert is a plot of XPS spectrum of the Ti2p photoemission from Pt/TiO_2 (HF).

using Scherrer's equation from the full-width half-maximum of the Pt (1 1 1) peak:

$$d(\text{Å}) = \frac{k\lambda}{\beta \cos\theta} \quad (2)$$

where d is the average particle size (Å), k is the shape-sensitive coefficient (0.9), λ is the wavelength of radiation used (1.54056 Å), β is the full-width half-maximum (in rad) of the peak, and θ is the angle at the position of peak maximum (in rad). All the diffraction peaks overlapped between 40° of Pt (1 1 1) and 41° of TiO_2 (1 1 1). The

Table 1
Distribution of Ti species and relative intensities in Pt/TiO_2 samples.

Sample	Assigned chemical state	Binding energy (eV)	Relative intensity (%)
Pt/TiO_2 (non)	Ti(IV)	458.22	36.4
	Ti(III)	456.3	30.2
	Ti(II)	–	–
Pt/TiO_2 (urea)	Ti(IV)	458.3	33.1
	Ti(III)	457.17	15.8
	Ti(II)	454.36	17.7
Pt/TiO_2 (thiourea)	Ti(IV)	458.18	41.9
	Ti(III)	456.71	12.5
	Ti(II)	454.38	12.3
Pt/TiO_2 (HF)	Ti(IV)	458.06	32.5
	Ti(III)	456.48	23.5
	Ti(II)	454.38	10.7

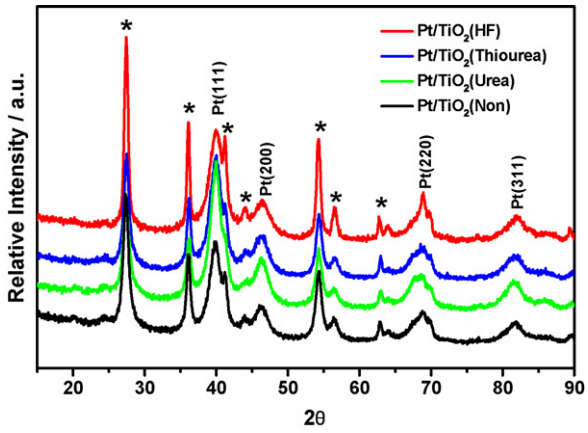

Fig. 5. X-ray diffraction patterns of the various Pt/TiO_2 catalysts. (*) Represents XRD patterns of the TiO_2 rutile nanosized support.

Table 2
Average particle size of catalysts from XRD data of Fig. 5.

Catalyst	Average particle size (nm)	Surface area ($m^2\,g^{-1}$)
Pt/TiO_2 (non)	6.05	46.3
Pt/TiO_2 (urea)	4.52	62.0
Pt/TiO_2 (thiourea)	4.17	67.2
Pt/TiO_2 (HF)	3.64	77.0

peak of 40° of Pt (1 1 1) was only calculated using the Lorentzian. The surface area (SA) platinum of the catalyst can be calculated, assuming homogeneously distributed and spherical particles, by the following equation:

$$\text{SA} = \frac{4\pi r^2}{\rho \times (4/3)\pi r^3} = \frac{6 \times 000}{\rho d} \quad (3)$$

The surface area of platinum ($m^2\,g^{-1}$) can be calculated from the surface area of a spherical particle ($4\pi r^2$) over the mass of a spherical particle ($\rho \times 4/3\pi r^3$). d ($d = 2r$) is the average particle size of the platinum from the Eq. (2) and ρ is the density of Pt particles ($21.4\,g\,cm^{-3}$) [32,33]. Table 2 shows the average particle size of Pt and the surface area of Pt. It was identified through the XRD data that the platinum nanoparticles of the additive-treated TiO_2 samples were smaller, and the surface area was higher, than Pt/TiO_2 (non) samples. Notably, Pt/TiO_2 (HF) had the smallest size of Pt and the largest surface area among the additive treated samples.

Cyclic voltammograms were employed to obtain the electrochemical surface area (ECSA) of Pt/TiO_2 electrocatalysts. Fig. 6 shows CV obtained in N_2-saturated 0.1 M $HClO_4$ at a scan rate of

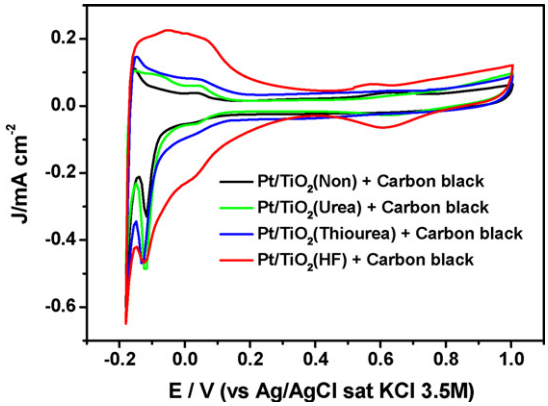

Fig. 6. Cyclic voltammograms of the various Pt/TiO_2 + carbon black electrocatalyst in N_2-saturated 0.1 M $HClO_4$ solution at a scan rate of 20 mV/s.

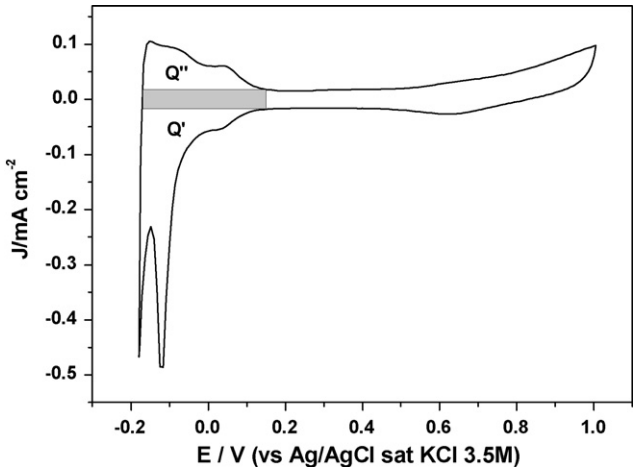

Fig. 7. Cyclic voltammograms of the Pt/TiO_2 (urea) + carbon black. Q' and Q'' represent the amount of charge exchanged during the electro-adsorption and desorption of H_2 on Pt sites. The gray-filled rectangular area is an estimate of the charge contribution from Pt double-layer charging and the capacitance of the support.

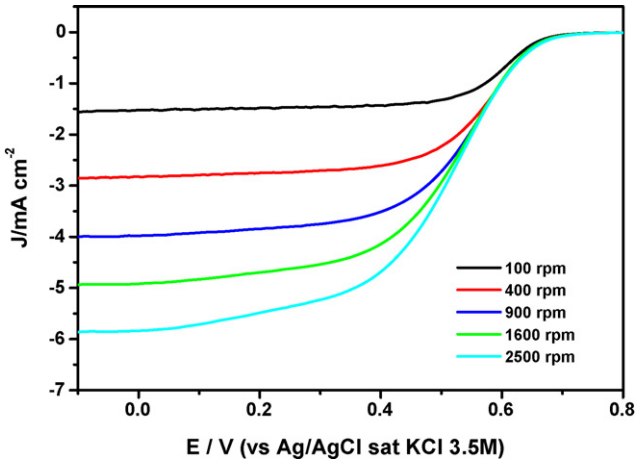

Fig. 8. Polarization curves of Pt/TiO_2 (HF) + carbon black electrocatalysts in oxygen-saturated 0.1 M $HClO_4$ solution at various rotating speeds from 100 to 2500 rpm with a scan rate of 5 mV/s.

20 mV/s for the different additives used in the Pt/TiO_2 samples. In this study, we used carbon black as conductor materials because, although the band gap of TiO_2 was decreased by shape change, the electronic conductivity was still insufficient to apply to electrocatalyst supports. The columbic charge for hydrogen desorption (Q_H) was used to calculate the active surface of the electrode. Among the samples, the CV of Pt/TiO_2 (urea) + carbon black are representatively shown in Fig. 7. The value of Q_H was calculated by taking the mean value between the amounts of charge exchanged during the electro-adsorption (Q') and desorption (Q'') of H_2 on the platinum sites [34]. The gray-filled rectangular area, which is an estimate of the charge contribution from Pt double-layer charging and the capacitance of the support, was evaluated for every sample, as shown in Fig. 7.

The charges of Q', Q'', Q_H and ECSA are summarized in Table 3. The ECSA was calculated as follows [33]:

$$\mathrm{ECSA} = \frac{Q_H}{[\mathrm{Pt}] \times 0.21} \tag{4}$$

where [Pt] is the platinum loading (25.48 $\mu g\,cm^{-2}$) in the electrode, Q_H is the charge for the hydrogen desorption ($mC\,cm^{-2}$), and 0.21 ($mC\,cm^{-2}$) is the charge required to oxidize a monolayer of H_2 on platinum [35]. Additive-treated TiO_2 samples, especially Pt/TiO_2 (HF), showed the better ECSA because of the high dispersion of Pt particles compared to Pt/TiO_2 (non), as can be also identified in TEM images (Fig. 1).

To estimate the electrocatalytic activity for ORR, TF-RDE technique was adopted. Fig. 8 shows polarization curves of Pt/TiO_2 (HF) + carbon black electrocatalysts in oxygen-saturated 0.1 M $HClO_4$ solution at various rotating speeds from 100 to 2500 rpm with a scan rate of 5 mV/s. As can be seen in Fig. 9(a), Pt/TiO_2 (HF) demonstrated the best ORR activity, while other samples showed insufficient performance to apply them to cathode electrocatalysts. This is because only HF treated TiO_2 supports have an improved electronic characteristics on the surface due to the narrowed band gap. It is interesting to note that the order of ORR activity in various samples is in accordance with the band gap narrowing, in the following sequence: Pt/TiO_2 (non) + carbon black < Pt/TiO_2 (urea) + carbon black < Pt/TiO_2 (thiourea) + carbon black < Pt/TiO_2 (HF) + carbon black. Therefore, the most important factor to decide the ORR activity for electrocatalysts supported on oxide semiconductor materials is the surface electronic characteristics of supports which is determined by the band gap.

The measured electrode current densities at different constant potentials were applied to the Koutecky–Levich plot. Fig. 9(b) represents the inverse current (j^{-1}) as a function of the inverse of the square root of the rotation rate ($\omega^{-1/2}$); i.e., the so-called Koutecky–Levich plot [36]:

$$\frac{1}{J} = \frac{1}{J_K} + \frac{1}{J_{\mathrm{diff}}} = \frac{1}{J_K} + \frac{1}{B\omega^{1/2}} \tag{5}$$

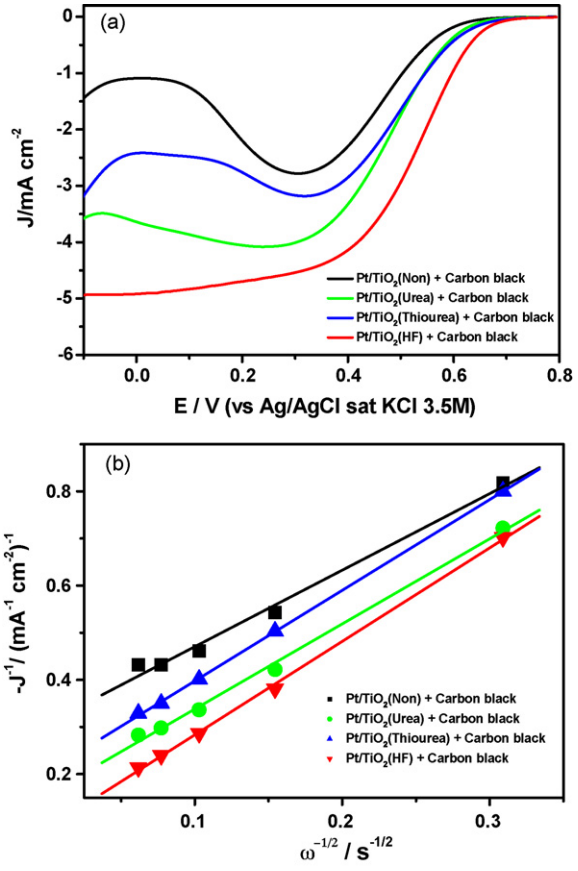

Fig. 9. ORR (a) of the various Pt/TiO_2 + carbon black electrocatalysts in oxygen-saturated 0.1 M $HClO_4$ solution at a rotating speed of 1600 rpm and scan rate of 5 mV/s. Koutecky–Levich plots (b) for ORR on the various Pt/TiO_2 + carbon black electrocatalysts at 0.4 V.

Table 3
Hydrogen adsorption and desorption charges, mean values, and electrochemical active surface (EAS) for different additives used.

Catalyst	Q' (mC cm^{-2})	Q'' (mC cm^{-2})	Q_H (mC cm^{-2})	Q_H/[Pt] (mC mg^{-1})	EAS (m^2 g^{-1})
Pt/TiO_2 (non)	5.292	1.609	3.451	135.4	664.8
Pt/TiO_2 (urea)	12.70	5.357	9.029	354.4	1686
Pt/TiO_2 (thiourea)	8.076	2.695	5.386	211.4	1007
Pt/TiO_2 (HF)	17.06	9.720	13.39	525.5	2502

in which

$$B = \frac{0.62nFC_0D_0^{2/3}}{\eta^{1/6}} \quad (6)$$

where J_K is the kinetic current, J_{diff} is the diffusion limiting current, n is the number of electrons transferred, F is Faraday's constant (F = 96485.3399 C/mol), C_0 is the O_2 concentration in the electrolyte ($C_0 = 1.26 \times 10^{-3}$ mol/l), D_0 is the diffusion coefficient of O_2 in the $HClO_4$ solution ($D_0 = 1.93 \times 10^{-5}$ cm^2/s), and η is the viscosity of the electrolyte ($\eta = 1.009 \times 10^{-2}$ cm^2/s) [37]. The slope of the inset plot (J^{-1} vs. $\omega^{-1/2}$) is $1/B$. By determining B factor, the number of electrons involved in the ORR can be obtained. The number of transferred electrons of Pt/TiO_2 (non), Pt/TiO_2 (urea), Pt/TiO_2 (thiourea), Pt/TiO_2 (HF) with carbon black were found to be 2.73, 3.04, 3.24, and 3.33 respectively. We can therefore conclude that the additive treatment of TiO_2, especially HF-treatment, leads to more facile kinetics closed to the four electron ORR pathway by decreasing the band gap and the higher ECSA of Pt nanoparticles. The absolute value of transferred electron, namely, ORR kinetics is however still much lower than the electrocatalysts using carbon supports, implying that the improved electronic properties of TiO_2 by shape change are still insufficient to directly apply to electrocatalyst supports. However, we firmly believe that if we fully understand the mechanism to decrease the band gap and optimize the shape change process with more studies, it is possible to develop superior oxide supports for electrocatalysts having an improved electronic characteristics and enhanced durability, compared to carbon supports.

4. Conclusions

Although the oxide materials are considered as alternative supports to overcome the carbon corrosion problem in PEMFC, the intrinsic semiconductor properties are the hurdle to apply them to actual electrocatalyst supports. To solve this problem, we introduced a unique method to decrease band gap by shape control using hydrothermal treatment with various additives. The additive-treated TiO_2 supports affected the size and the dispersion of Pt particles, and changed the surface area, which could be identified by TEM, XRD, and CV. Pt electrocatalysts supported on HF-treated TiO_2 exhibited the highly enhanced ORR activity compared to the other samples because of the narrowed band gap based on the existence of Ti^{2+} and Ti^{3+} which act as a donor. The HF treatment is therefore one of promising approach which enables us to employ TiO_2 as electrocatalyst supports by improving electronic characteristics.

Acknowledgment

This work was supported by the Korea Research Foundation Grant (KRF-2008-331-D00094) funded by the Korean Government (MOEHRD) and the second phase of the Brain Korea 21 Program in 2008.

References

[1] J. Larminie, A. Dicks, Fuel Cell Systems Explained, second edition, John Wiley & Sons, 2003.
[2] Y. Shao-Horn, W.C. Sheng, S. Chen, P.J. Ferreira, E.F. Holby, D. Morgan, Topics in Catalysis 46 (2007) 285.
[3] V.R. Stamenkovic, B. Fowler, B.S. Mun, G.F. Wang, P.N. Ross, C.A. Lucas, N.M. Markovic, Science 315 (2007) 493.
[4] C. Dupont, Y. Jugnet, D. Loffreda, Journal of the American Chemical Society 128 (2006) 9129.
[5] Y. Xu, A.V. Ruban, M. Mavrikakis, Journal of the American Chemical Society 126 (2004) 4717.
[6] Y.Y. Tong, H.S. Kim, P.K. Babu, P. Waszczuk, A. Wieckowski, E. Oldfield, Journal of the American Chemical Society 124 (2002) 468.
[7] X.W. Yu, S.Y. Ye, Journal of Power Sources 172 (2007) 145.
[8] B. Lei, J.J. Xue, D.P. Jin, S.G. Ni, H.B. Sun, Rare Metals 27 (2008) 445.
[9] J. Shim, C.R. Lee, H.K. Lee, J.S. Lee, E.J. Cairns, Journal of Power Sources 102 (2001) 172.
[10] M. Wang, D.J. Guo, H.L. Li, Journal of Solid State Chemistry 178 (2005) 1996.
[11] T. Ioroi, Z. Siroma, N. Fujiwara, S. Yamazaki, K. Yasuda, Electrochemistry Communications 7 (2005) 183.
[12] X.Z. Cui, J.L. Shi, H.R. Chen, L.X. Zhang, L.M. Guo, J.H. Gao, J.B. Li, Journal of Physical Chemistry B 112 (2008) 12024.
[13] S.H. Kang, T.Y. Jeon, H.S. Kim, Y.E. Sung, W.H. Smyrl, Journal of the Electrochemical Society 155 (2008) B1058.
[14] S.H. Kang, Y.E. Sung, W.H. Smyrl, Journal of the Electrochemical Society 155 (2008) B1128.
[15] K.S. Lee, I.S. Park, Y.H. Cho, D.S. Jung, N. Jung, H.Y. Park, Y.E. Sung, Journal of Catalysis 258 (2008) 143.
[16] K.W. Park, K.S. Seol, Electrochemistry Communications 9 (2007) 2256.
[17] K. Drew, G. Girishkumar, K. Vinodgopal, P.V. Kamat, Journal of Physical Chemistry B 109 (2005) 11851.
[18] M. Hepel, I. Kumarihamy, C.J. Zhong, Electrochemistry Communications 8 (2006) 1439.
[19] J.M. Macak, P.J. Barczuk, H. Tsuchiya, M.Z. Nowakowska, A. Ghicov, M. Chojak, S. Bauer, S. Virtanen, P.J. Kulesza, P. Schmuki, Electrochemistry Communications 7 (2005) 1417.
[20] F. Peng, L.F. Cai, H. Yu, H.J. Wang, J. Yang, Journal of Solid State Chemistry 181 (2008) 130.
[21] J.A. Tian, G.Q. Sun, L.H. Jiang, S.Y. Yan, Q. Mao, Q. Xin, Electrochemistry Communications 9 (2007) 563.
[22] M. Gratzel, Nature 414 (2001) 338.
[23] S. Horikoshi, H. Hidaka, N. Serpone, Chemical Physics Letters 376 (2003) 475.
[24] Q.H. Zhang, L. Gao, J.K. Guo, Journal of the European Ceramic Society 20 (2000) 2153.
[25] R. Beranek, H. Hildebrand, P. Schmuki, Electrochemical and Solid-State Letters 6 (2003) B12.
[26] J.M. Macak, K. Sirotna, P. Schmuki, Electrochimica Acta 50 (2005) 3679.
[27] J.W. Tang, Z.G. Zou, J.H. Ye, Research on Chemical Intermediates 31 (2005) 505.
[28] Y. Cong, J.L. Zhang, F. Chen, M. Anpo, Journal of Physical Chemistry C 111 (2007) 6976.
[29] J.C. Yu, L.Z. Zhang, Z. Zheng, J.C. Zhao, Chemistry of Materials 15 (2003) 2280.
[30] A.M. More, J.L. Gunjkar, C.D. Lokhande, R.S. Mane, S.H. Han, Micron 38 (2007) 500.
[31] G. Guisbiers, O. Van Overschelde, M. Wautelet, Applied Physics Letters 92 (2008).
[32] S.P. Jiang, Z.C. Liu, H.L. Tang, M. Pan, Electrochimica Acta 51 (2006) 5721.
[33] A. Pozio, M. De Francesco, A. Cemmi, F. Cardellini, L. Giorgi, Journal of Power Sources 105 (2002) 13.
[34] T.J. Schmidt, H.A. Gasteiger, G.D. Stab, P.M. Urban, D.M. Kolb, R.J. Behm, Journal of the Electrochemical Society 145 (1998) 2354.
[35] J. Perez, E.R. Gonzalez, E.A. Ticianelli, Electrochimica Acta 44 (1998) 1329.
[36] M.H. Shao, T. Huang, P. Liu, J. Zhang, K. Sasaki, M.B. Vukmirovic, R.R. Adzic, Langmuir 22 (2006) 10409.
[37] J. Zhang, Y. Mo, M.B. Vukmirovic, R. Klie, K. Sasaki, R.R. Adzic, Journal of Physical Chemistry B 108 (2004) 10955.